LA-UR - 90-4214

CONF-9010286--1

JAN 08 1991

LA-UR--90-4214

DE91 005881

Los Alamos National Laboratory is operated by the University of California for the United States Department of Energy under contract W-7405-ENG-36

TITLE: THE NONLINEAR SCHRODINGER EQUATION ON A DISORDERED CHAIN

AUTHOR(S): Rainer Scharf
A. R. Bishop

SUBMITTED TO: Springer Proceedings in Physics "Nonlinearity with Disorder"
International Workshop, Tashkent, USSR, October 1-7, 1990

DISCLAIMER

This report was prepared as an account of work sponsored by an agency of the United States Government. Neither the United States Government nor any agency thereof, nor any of their employees, makes any warranty, express or implied, or assumes any legal liability or responsibility for the accuracy, completeness, or usefulness of any information, apparatus, product, or process disclosed, or represents that its use would not infringe privately owned rights. Reference herein to any specific commercial product, process, or service by trade name, trademark, manufacturer, or otherwise does not necessarily constitute or imply its endorsement, recommendation, or favoring by the United States Government or any agency thereof. The views and opinions of authors expressed herein do not necessarily state or reflect those of the United States Government or any agency thereof.

By acceptance of this article, the publisher recognizes that the U S Government retains a nonexclusive, royalty-free license to publish or reproduce the published form of this contribution or to allow others to do so, for U S Government purposes.

The Los Alamos National Laboratory requests that the publisher identify this article as work performed under the auspices of the U S Department of Energy

Los Alamos Los Alamos National Laboratory
Los Alamos, New Mexico 87545

FORM NO 836 R4
ST NO 2629 5/81

DISTRIBUTION OF THIS DOCUMENT IS UNLIMITED

MASTER

The nonlinear Schrödinger equation on a disordered chain

Rainer Scharf and A. R. Bishop

Theoretical Division and Center for Nonlinear Studies, Los Alamos National Laboratory, Los Alamos, NM 87545, USA

The integrable lattice nonlinear Schrödinger equation is a unique model with which to investigate the effects of disorder on a discrete integrable dynamics, and its interplay with nonlinearity. We first review some features of the lattice nonlinear Schrödinger equation in the absence of disorder and introduce a 1- and 2-soliton collective variable approximation. Then we describe the effect of different types of disorder: attractive and repulsive isolated impurities, spatially periodic potentials, random potentials, and time dependent (kicked) long wavelength perturbations.

1. Introduction

Recent years have seen an enormous progress in understanding the effects of disorder in linear systems like Anderson localization and the transition from insulating to conducting behavior in $d = 3$ dimensions at zero temperature upon decreasing the disorder. Completely integrable nonlinear systems in $d = 1$ are also fairly well understood by now. The understanding of the interplay between disorder and nonlinearity on the other hand is still in its infancy [1].

Both, nonlinearity and disorder, may give rise to self-localized excitations (solitons or Anderson localized wave packets, respectively). Therefore it is natural to ask, how these effects might reinforce, complement or frustrate each other. Transport properties in disordered, nonlinear materials for example strongly depend on whether solitons behave as "particles" in the presence of disorder, or interact very strongly with other degrees of freedom. Does the nonlinearity lead to adaptive behavior of excitations in disordered materials which preserves coherence? How do nonlinear excitations interact with each other in the presence of disorder? These and other issues are of great experimental concern in fields from nonlinear optics [2], to polaron formation in solid state materials [3,4], to vibron localization in natural and synthetic biomolecules [5,6,7].

In all the cases mentioned so far perturbation theory allows us to calculate which of the unperturbed structures becomes unstable and how they start to decay [8]. But it does not tell us, what excitations in fully developed disorder look like. Collective variable approximations together with numerical experiments allow us to investigate these properties in greater detail.

As a first step, in this rich program, we consider the *discrete* nonlinear Schrödinger equation (NLS eq.) in $(1 + 1)$ dimensions and investigate some

elementary forms of parametric spatial and time periodic disorder – namely constant bias, isolated impurities, periodic and random spatial variations, and time periodic (kicked) perturbations. Several novel features have been found, some of them being a result of the spatial discreteness of the dynamics.

2. The completely integrable lattice NLS equation

Ablowitz and Ladik [9] have introduce a completely integrable discretization of the NLS equation. We generalize it by including an onsite potential energy term:

$$i\dot{\psi}_n = -(\psi_{n+1} + \psi_{n-1})(1 - \kappa|\psi_n|^2) + V_n\psi_n, \tag{1}$$

with $\kappa = -1$ or $+1$ (attractive or repulsive self-interaction, respectively). This equation can be derived from the Hamiltonian

$$H = -\sum_n (\psi_n\psi^*_{n+1} + \psi^*_n\psi_{n+1}) - \frac{1}{\kappa}\sum_n V_n \log(1 - \kappa|\psi_n|^2), \tag{2}$$

with nonstandard Poisson brackets

$$\{\psi_m, \psi^*_n\} = i(1 - \kappa|\psi_n|^2)\delta_{mn}, \qquad \{\psi_m, \psi_n\} = \{\psi^*_m, \psi^*_n\} = 0, \tag{3}$$

and $\kappa = \pm 1$. For $\kappa = 1$ we assume $|\psi_n| < 1$. One can easily verify that the following "norm" is conserved:

$$N = -\frac{1}{\kappa}\sum_n \log(1 - \kappa|\psi_n|^2). \tag{4}$$

We now show that eq. (1) is completely integrable, not only for constant $V_n = V$, but also in the case $V_n = an + b$ with $a \neq 0$. To accomplish this we cast eq. (1) in the form af a zero curvature condition with time-dependent spectral parameter λ. Following ref. 10, the compatibility condition for a vector $F_n(t, \lambda(t))$ obeying the equations

$$\begin{aligned} F_{n+1} &= L_n(t,\lambda)\, F_n, \\ \frac{dF_n}{dt} &= W_n(t,\lambda)\, F_n, \end{aligned} \tag{5}$$

is of the following form:

$$\frac{d}{dt}L_n + L_nW_n - W_{n+1}L_n = 0. \tag{6}$$

With the choice

$$\begin{aligned} L_n(t,\lambda) &= \begin{pmatrix} \lambda & \sqrt{\kappa}\psi^*_n \\ \sqrt{\kappa}\psi_n & \lambda^{-1} \end{pmatrix}, \\ W_n(t,\lambda) &= i\begin{pmatrix} 1 + \kappa\psi^*_n\psi_{n-1} - \lambda^2 + f_n & \sqrt{\kappa}(\lambda^{-1}\psi^*_{n-1} - \lambda\psi^*_n) \\ \sqrt{\kappa}(\lambda^{-1}\psi_n - \lambda\psi_{n-1}) & -1 - \kappa\psi_n\psi^*_{n-1} + \lambda^{-2} - f_n \end{pmatrix}, \end{aligned} \tag{7}$$

the zero curvature condition (6) leads to eq. (1) with

$$\begin{aligned} f_n &= \gamma n + \delta, \\ \lambda(t) &= \lambda_0 e^{i\gamma t}, \\ V_n &= 2 + f_n + f_{n+1} = 2\gamma n + 2(\delta + 1) + \gamma = an + b. \end{aligned} \tag{8}$$

In the case of periodic boundary conditions, for example, a hierarchy of (time dependent for $V_n = an + b$) integrals of motion may be constructed from the trace of powers of the (2×2)-matrix

$$L = L_M L_{M-1} \dots L_2 L_1, \tag{9}$$

with $L_{M+1} \equiv L_1$. For example, $\log|\det L|$ leads to the norm N, whereas $\operatorname{tr} L$ lead to the kinetic part of the Hamiltonian H.

3. Constant and linear onsite potentials

In what follows we will always assume attractive self-interaction and set $\kappa = -1$. For $V_n \equiv V$ or $V_n = an + b$ travelling solutions exist and can be expressed in terms of elliptic functions. Of special interest are the 1-soliton solutions. For $V_n \equiv V$ they are of the form

$$\begin{aligned} \psi_n(t) &= \sinh\beta \, \operatorname{sech}\big(\beta(n - ut - x_0)\big) \, e^{-i(\omega t + \alpha n + \phi_0)}, \\ \omega &= -2\cosh\beta \, \cos\alpha + V, \\ u &= -\frac{2\sinh\beta \, \sin\alpha}{\beta}. \end{aligned} \tag{10}$$

The existence of a maximum velocity $u_{\max} = 2\sinh\beta/\beta$ is clearly a discreteness effect. Energy and norm for the 1-soliton solution (10) are found to be

$$\begin{aligned} E &= -4\sinh\beta \, \cos\alpha, \\ N &= 2\beta. \end{aligned} \tag{11}$$

For $V_n = an + b$ the solitons have the same shape but move in a different manner (with $\alpha_0 = \phi_0 = 0$ for simplicity):

$$\begin{aligned} \psi_n(t) &= \sinh\beta \, \operatorname{sech}\big(\beta(n - x(t))\big) \, e^{-i(\phi(t) + V_n t)}, \\ \phi(t) &= -\frac{2}{a}\cosh\beta \, \sin(at) + bt, \\ x(t) &= \frac{2}{a\beta}\sinh\beta \, \big(\cos(at) - 1\big) + x_0. \end{aligned} \tag{12}$$

The solitons move exactly harmonically in a linear potential (see Fig. 1). Their norm is unchanged, $N = 2\beta$, but their energy is given by

$$\begin{aligned} E &= -4\sinh\beta\cos(at) + 2\beta(ax(t) + b) \\ &= -4\sinh\beta + 2\beta(ax_0 + b). \end{aligned} \tag{13}$$

The explicit 2-soliton solutions are, as usual, quite involved. Therefore we only show the collision of two different solitons for $V_n = an + b$ in Fig. 2, thereby illustrating the complete integrability in this case. In the continuum limit the NLS eq. is also integrable for harmonic potentials [11]. Whether this is also true in the discrete case seems to be unknown.

4. The 1-soliton collective variable approximation

As noted above, in the case of a linear potential solitons move in a harmonic way without changing their shape. This is no longer true for a more general form of the potential. But as long as the curvature of the potential felt by the soliton is small one might assume that the soliton emits only a negligeable amount of radiation and adjusts its parameters to comply with the constancy of energy and norm. Introducing $V(x)$ for $V_n(n = x)$, this lead to $N = 2\beta$ being independent of $V(x)$ and

$$E = -4\sinh\beta\,\cos\alpha(x) + 2\beta V(x) = \text{const.} \tag{14}$$

Now x is interpreted as the position of the soliton, the relevant collective variable. The soliton might be regarded as a particle moving in an effective potential with a velocity $u(x) = -2\sinh\beta\sin\alpha/\beta$:

$$\frac{u^2}{2} + \frac{V(x)(\beta V(x) - E)}{2\beta} = \frac{16\sinh^2\beta - E^2}{8\beta^2}, \tag{15}$$

where $V_{\text{eff}}(x) = \frac{1}{2\beta}V(x)(\beta V(x) - E)$ plays the role of the effective potential and the r. h. s. of eq. (15) plays the role of the particle energy, both depending on the initial conditions. A constant potential V leads to a constant effective potential $V_{\text{eff}}(x)$, a linear potential $V(x)$ lead to a harmonic $V_{\text{eff}}(x)$.

That the effective potential $V_{\text{eff}}(x)$ is the relevant one and not the original potential $V(x)$ can be seen in Fig. 3, which shows the trapping of a soliton on a *maximum* of $V(x)$!

Solitons trying to percolate on a onedimensional lattice in a smooth random potential with small curvature have to observe not only a lower bound for their energy, but also an upper one. There exist lower and upper bounds for the potential that the soliton is allowed to enter without being reflected, depending on the initial condition ($E = -4\sinh\beta\,\cos\alpha_0 + 2\beta V_0$):

$$\begin{aligned} V_{\text{max}} - V_0 &= \frac{2\sinh\beta}{\beta}(1 - \cos\alpha_0), \\ V_0 - V_{\text{min}} &= \frac{2\sinh\beta}{\beta}(1 + \cos\alpha_0). \end{aligned} \tag{16}$$

This window of allowed potential values acts as a filter for solitons having certain initial values for α and β, as long as the collective variable approximation holds. In the continuum limit the unusual lower bound disappears.

5. Trapping on an impurity

The case of an isolated single impurity of the form $V_n = V\,\delta_{n,0}$ is important in two respects. First it illustrates that the stationary solutions do *not* tell the full story of what is going on in the system, as opposed to the case of the linear Schrödinger equation; and second it shows that a collective variable approach can be useful even in the case when one soliton breaks in two.

Stationary solutions with the frequency $\omega = -2\cosh\beta$ are readily found to be of the form

$$\psi_n(t) = \sinh\beta\,\mathrm{sech}\big(\beta(|n| - \mathrm{sgn}(V)\xi)\big)\,e^{-i\omega t}, \tag{17}$$

where $\xi > 0$ and $\cosh\beta\xi = 2\sinh\beta/\sqrt{\omega^2 - 4 - V^2}$. For an attractive impurity ($V < 0$) the solution ψ_n has a maximum at $n = 0$; for a repulsive impurity ($V > 0$) it has a minimum at $n = 0$ between maxima at $\pm n_0 \approx \xi$. For $V = 0$ the original soliton with $\xi = 0$ is recovered. In all cases solutions (17) exist only for sufficiently large β: $\sinh\beta \geq |V|/2$.

What really happens dynamically in the vicinity of an impurity might look quite different from the trapped oscillatory solution (17). There may be scattering and emission of phonon-like excitations as well as multi-soliton processes. To simplify matters we choose a soliton at rest ($\alpha = 0$) on top of the impurity and assume that the main decay channel is through generation of two solitons. As the initial condition is symmetric with respect to spatial inversion, we expect the two solitons to have the same shape but opposite velocity. Initially we have for the norm: $N = 2\beta$, and for the energy: $E = -4\sinh\beta + 2V\log(\cosh\beta)$. Well after the decay into 2 travelling solitons (and hopefully negligeable radiation) with exponentially small overlap with the impurity we find for the norm $N' = 4\beta'$, and for the energy $E' = -8\sinh\beta'\cos\alpha'$. If we assume that the amount of radiation emitted during the decay is negligeable ($N = N'$, $E = E'$) we find:

$$\cos\alpha' = \cosh(\beta/2) - \frac{V\log(\cosh\beta)}{4\sinh\frac{\beta}{2}}. \tag{18}$$

This equation has solutions for α' only if V falls into the following interval:

$$0 < \frac{4\sinh\frac{\beta}{2}\left(\cosh\frac{\beta}{2} - 1\right)}{\log(\cosh\beta)} < V < \frac{4\sinh\frac{\beta}{2}\left(\cosh\frac{\beta}{2} + 1\right)}{\log(\cosh\beta)}. \tag{19}$$

In the continuum limit these bounds got to 0 and $+\infty$. The upper bound in eq. (19) corresponds to a relatively strong potential for which more complicated things are expected to happen than only 2-soliton decay without radiation. The lower bound on the other hand is small for small β and our ansatz is reasonable in this case. We therefore expect bound states for potentials V smaller than the lower bound in eq. (19) — even if V is repulsive! Fig. 4 shows how a soliton at rest centered at an isolated attractive impurity adjusts and stays trapped.

Fig. 5 illustrates the same but for a repulsive impurity below the critical value V_c for soliton breakup (the lower bound in eq. (19)). Fig. 6 shows the breakup into two unbound solitons. The actual value for V_c is about 10% higher than the one given by eq. (19) because of radiative losses, reducing the kinetic energy available for the emerging solitons.

It is interesting to compare V_c here with the crossover suggested in disordered "polaron" problems (with electron-phonon, exciton-phonon, magnon-phonon coupling) discussed by Anderson [12] and others [13]. These authors have considered the competition of disorder- and nonlinearity-induced localization within a stationary approximation ($\psi_n(t) = \exp(-i\omega t)\chi_n$), whereas here we have explored the full time-dependence.

6. Spatially periodic onsite potentials

If a soliton experiences a spatially periodic onsite potential one crucial parameter that governs its behavior is the ratio between the width of the soliton and the modulation length of the potential. The other is the ratio between the soliton amplitude $\max_n |\psi_n|^2$ and the amplitude of the potential. Let's start with the latter. If this ratio is large then the nonlinearity effects dominate. In the opposite case the soliton is expected to decay into different coherent structures centered around the minima of the potential. But what is going to happen exactly will be governed by the lengthscale ratio mentioned first. If the soliton is narrow compared to the wavelength of the potential then it will essentially move like a particle in an effective potential, as described in section 4. If the soliton is broad compared to the wavelength of the potential and it moves sufficiently fast then a smoothing over the potential is likely to occur and the soliton will only feel a reduced effective potential. A situation of major physical interest is when nonlinearity and onsite perturbation or width of the soliton and wavelength of the perturbation are comparable: then a breakdown of a simple particle (soliton) picture can be anticipated, corresponding to strong scattering. Thus the periodic potential is very important for understanding disorder of general color.

In Fig. 7 we illustrate the case of a broad soliton ($\beta = 0.1$) slowly moving ($\alpha = 0.5$) in a periodic potential. The period of the potential is comparable to the width of the soliton, the amplitude of the potential is comparable to the height of the soliton. It is clearly visible that the soliton steepens up each time it encounters a maximum of the potential. It tries to adjust as it travels over the wiggles but is able to do so only in an imperfect manner: it leaves behind some excitations which get trapped in the minima of the potential. If the soliton moves even more slowly initially ($\alpha = 0.3$) it decays rapidly into a couple of humps which stay trapped in the potential minima. On the other hand if the soliton moves very fast ($\alpha = 1.57$) it smoothes over the potential and is not visibly affected by it. One way to interprete these results is in terms of excitation of shape modes. If the soliton moves slowly enough over the wiggler potential there is strong excitation of shape modes, besides other excitations

which are left behind and get trapped. But for sufficiently large velocity of the soliton and correspondingly higher wiggler frequency the excitation of shape modes of that frequency is strongly reduced. A detailed stability analysis of the shape modes is in progress. The interplay between the characteristic frequency ω of the unperturbed soliton, the frequency of the shape mode oscillation, and the wiggler frequency might give rise to phenomena well known from the circle map, as, for example, mode locking, and chaos.

7. Spatially random onsite potentials

Of major interest is the case of a single soliton travelling along a disordered chain. Several questions arise in this case: What are the radiative losses the soliton suffers? How far does the soliton travel before it decays? How does the mean velocity of the soliton depend on the strength of the disordered potential? Will the emitted radiation become Anderson localized ? Will it self-focus into new solitons?

We have investigated how one or two broad solitons ($\beta \ll 1$) travel in a random onsite potential V_n equally distributed in the interval $[-V, V]$. Slowly travelling solitons in weak potentials decay rapidly and are soon overtaken by the radiation they generate. Fast solitons on the other hand stay ahead of their radiation for a longer time and — which seems to be more important — they dynamically smooth out the random potential. This is quite similar to the case of periodic potentials as shown in sect. 6. Strong fluctuations in the potential give rise to modulations in the shape of the soliton, which become more pronounced the longer it takes for the soliton to pass over the fluctuations. The modulations of the soliton shape are finally left behind as excitations travelling in the opposite direction with about the same velocity as the soliton. The velocity of a broad soliton travelling in a small random potential is essentially unchanged in comparison to its value without disorder: $u \approx -2 \sin \alpha$. The radiation front which the soliton generates travels with a maximum velocity $u_0 \approx 2$. Therefore only solitons with $\alpha \approx \pi/2$ stay ahead of their own radiation for a sufficiently long time.

We also investigated the case of two identical solitons, travelling in the same direction with a separation of a few soliton widths. The soliton that travelled in the wake of the leading one was only negligeably influenced by the wake. The superposition of the wakes of both solitons contained more pronounced structures than each of the wakes alone, as is to be expected because of the self-focussing nonlinearity. The ultimate fate of the structures and the radiation that is left behind is still unclear — whether the structures decay into radiation which in turn then Anderson localizes, or whether the structures that are to small for nonlinearity to have any effect are "recycled" by larger structures. Whatever happens will be interesting to understand as it will involve the full timedependence of the nonlinear dynamics with disorder and not only properties of noninteracting stationary solutions [14].

Recently Newell and coworkers gave an account of their work on the trans-

mission properties of the nonlinear Schrödinger chain with disorder [15]. They show that the transmission properties are only improved by the nonlinearity if it contributes to self-focussing into soliton pulses.

8. The periodically kicked NLS chain

The different kinds of disorder we introduced so far were time independent. Now we allow for a periodical driving of a NLS chain with periodic boundary conditions ($\psi_{M+n} = \psi_n$). We choose a driving which facilitates the analysis in terms of a 1-soliton collective variable approximation, namely time periodic δ-kick perturbation:

$$i\dot{\psi}_n = -(\psi_{n+1} + \psi_{n-1})(1 + |\psi_n|^2) + KV_n\psi_n \sum_{m=-\infty}^{+\infty} \delta(t - mT) \qquad (20)$$

with $V_{n+M} = V_n$. The continuum limit of this equation for $V_n = \cos(2\pi n/M)$ was recently investigated by Casati and coworkers [16]. They found sensitive dependence of the time evolution on the initial conditions not only for single solitons, but also for more general initial conditions. For vanishing nonlinearity their model is equivalent to the quantum kicked rotor which shows dynamical localization in momentum representation — in striking contrast to the deterministic diffusion observed in the classical limit for sufficiently large kicking constant K The connection between this dynamical localization and Anderson localization in tight binding models was pointed out by Fishman, Grempel and Prange [17]. Casati and coworkers claim that the dynamical localization persists even in the case with nonlinearity, which certainly deserves further investigation.

We propose to use the discrete model (20) to investigate these questions in greater detail. Here we present some first results. We assume that the state of the chain is given at time $mT - 0$, i. e. immediately before the kick at time mT. Upon integrating eq. (20) from $mT - 0$ to $mT + 0$ one finds the following map

$$\psi_n(mT + 0) = \psi_n(mT - 0)\, e^{-iKV_n}. \qquad (21)$$

This map is succeeded by the completely integrable evolution from $mT + 0$ to $(m + 1)T - 0$, completing one iteration step. For the special case of a single, narrow soliton at time $mT - 0$ the effect of the kick can be calculated in 1-soliton collective variable approximation. Neglecting the unimportant overall phase factor ϕ_0 (see eq. (10)) the important soliton parameters are $x_0(t)$, $\alpha(t)$, and $\beta(t)$ with $t = mT$. Neglecting the curvature of V_n over the soliton hump we can approximate the kick by

$$\psi_n(mT + 0) = \psi_n(mT - 0)\, \exp^{-iK\left(V(x_0) + V'(x_0)(n - x_0)\right)}. \qquad (22)$$

Neglecting again overall phases this shows that x_0 and β are left unchanged by the kick: $x_0(mT+0) = x_0(mT-0)$ and $\beta(mT+0) = \beta(mT-0)$. The phase modulation α on the other hand does change:

$$\alpha(mT+0) = \alpha(mT-0) + KV'(x_0(mT-0)). \tag{23}$$

The integrable evolution between the kicks leaves β unchanged, too. Therefore β is an adiabatic invariant for the dynamics (20). The integrable evolution also leaves α, the velocity parameter, unchanged: $\alpha((m+1)T-0) = \alpha(mT+0)$. But the position of the soliton changes:

$$x_0((m+1)T-0) = x_0(mT+0) - \frac{2T\sinh\beta}{\beta}\sin\alpha(mT+0). \tag{24}$$

Now we introduce position and momentum variables, both ranging between 0 and 2π:

$$\begin{aligned} q_m &= \frac{2\pi}{M}x_0(mT-0), \\ p_m &= -\alpha(mT-0). \end{aligned} \tag{25}$$

With these new variables the soliton motion in 1-soliton collective variable approximation is described by a symplectic map:

$$\begin{aligned} p_{m+1} &= p_m - K\tilde{V}'(q_m), \\ q_{m+1} &= q_m + \tilde{T}(\beta)\sin(p_{m+1}), \end{aligned} \tag{26}$$

where $\tilde{V}(q_m) = V(x_0(mT-0))$ and $\tilde{T}(\beta) = 4\pi T\sinh\beta/M\beta$. For $\tilde{V}(q) = \cos q$ and in the region $|p| \ll 1$ the standard map is recovered. The full map then takes the doubly periodic form

$$\begin{aligned} p_{m+1} &= p_m + K\sin(q_m), \\ q_{m+1} &= q_m + T(\beta)\sin(p_{m+1}), \end{aligned} \tag{27}$$

with $T(\beta) = T(0)\sinh\beta/\beta$, upon skipping the wiggle. $T(\beta)$ takes into account that narrow solitons move faster than broad ones.

Eq. (27) is non-integrable for $KT(\beta) \neq 0$. For $K = T = 2$, for example (see Fig. 10), regions of regular and chaotic motion coexist. We place a single soliton in a regular region near an elliptic fixed point (Fig. 11, with q shifted by π in comparison with Fig. 10), and in a chaotic region near a hyperbolic fixed point (Fig. 12). The solitons display clearly different kinds of behavior. Fig. 13 shows that the motion of the soliton in the second case closely follows the chaotic classical iteration. Surprisingly it does so without breaking apart. The amount of radiation that is emitted is small and the shape of the soliton is practically unchanged.

Finally we address the question whether the dynamics of the chain is reversible and how this depends on the motion of the soliton. We monitor the spread of the soliton plus emitted radiation ($\sqrt{< q^2 > - < q >^2}$) over a number of time steps and then we time-reverse the dynamics. Because of inevitable numerical errors maps like the one given by eq. 27 are not reversible numerically over say 100 iterations for initial conditions with positive Lyapunov exponets. For the full dynamics of the chain (eq. (20)) integrated numerically with sufficiently large accuracy it turns out that the system returns to its initial condition upon time-reversal if the soliton is moving regularly (see Fig. 14). If the soliton is moving in a chaotic manner no available numerical accuracy was found to be sufficient to restore the initial conditions upon time-reversal. This illustrates the sensitive dependence of the dynamics on the initial condition if the soliton is started in a chaotic region. Our results clearly show that solitons can be forced to move chaotically with only negligeable excitation of other degrees of freedom.

Further interesting questions are for example: (i) how fast do solitons decay when the curvature of V_n is not negligeable; (ii) does the dynamics (20) show localization in p-direction when the corresponding map (26) shows deterministic diffusion (on the torus); (iii) how do two solitons interact in the presence of the kicking. These and further questions will be addressed in a forthcoming publication [18].

Acknowledgments

We thank F. Abdullaev, Y. Kivshar, P. Lomdahl, and D. Shepelyansky for valuable help and advice, and for support by the U. S. Department of Energy and NATO Grant RG674-88. Part of the work was done by one of us (R. S.) during a workshop on "Quantum aspects of nonlinear systems" at the Universität-GHS Essen which was sponsored by the European Science Foundation and the Sonderforschungsbereich "Unordnung und große Fluktuationen" of the Deutsche Forschungsgemeinschaft which is hereby gratefully acknowledged.

References

[1] A. R. Bishop, D. K. Campbell, and S. Pnevmatikos, eds, 1989, *Disorder and Nonlinearity* (Springer, Berlin)

[2] A. Hasegawa, 1989, *Optical Solitons in Fibers* (Springer, Berlin)

[3] N. Mott, 1987, *Conduction in Non-Crystalline Materials* (Oxford University Press, Oxford)

[4] A. L. Efros and M. Pollak, eds, 1985, *Electron-Electron Interaction in Disordered Systems* (North-Holland, Amsterdam)

[5] S. E. Trullinger, V. E. Zakharov, and V. L. Pokrovsky, eds, 1986, *Solitons* (North-Holland, Amsterdam)

[6] J. C. Eilbeck, P. S. Lomdahl, and A. C. Scott, 1985, *The discrete self-trapping equation*, Physica D **16**, 318-338

[7] A. C. Scott, 1985, *Davydov solitons in polypeptides*, Phil. Trans. R. Soc. Lond. A **315**, 423-436

[8] Y. S. Kivshar and B. A. Malomed, 1989, *Dynamics of solitons in nearly integrable systems*, Rev. Mod. Phys. **61**, 763-915

[9] M. J. Ablowitz and J. F. Ladik, 1976, *Nonlinear differential-difference equations and Fourier analysis*, J. Math. Phys. **17**, 1011-1018

[10] L. D. Faddeev and L. A. Takhtajan, 1987, *Hamiltonian Methods in the Theory of Solitons* (Springer, Berlin)

[11] R. Balakrishnan, 1985, *Soliton propagation in nonuniform media*, Phys. Rev. A **32**, 1144-1149

[12] P. W. Anderson, 1972, *Effect of Franck-Condon displacements on the mobility edge and the energy gap in disordered materials*, Nature **235**, 163-165

[13] M. H. Cohen, E. N. Economou, and C. M. Soukoulis, 1983, *Polaron formation near a mobility edge*, Phys. Rev. Lett. **51**, 1202-1205

[14] R. Scharf and A. R. Bishop, to be published

[15] J. G. Caputo, A. C. Newell, and M. Shelley, 1990, *Nonlinear wave propagation through a random medium and soliton tunneling*, preprint

[16] F. Benvenuto, G. Casati, A. S. Pikovsky, and D. L. Shepelyansky, 1990, *Manifestation of classical and quantum chaos in nonlinear wave propagation*, preprint

[17] S. Fishman, D. R. Grempel, and R. E. Prange, 1982, *Chaos, quantum recurrences, and Anderson localization*, Phys. Rev. Lett. **49**, 509-512

[18] R. Scharf, to be published

Figure captions

Fig. 1. *Soliton trapped on a tilted plane:* Solution of eq. (1), for $l_{\text{chain}} = 104$; zero boundary conditions; $V_n = 16n/l_{\text{chain}}$; initial soliton parameters: $\alpha = -1.571$, $\beta = 0.4$; integration time $T = 90$. The vertical marks indicate the turning points given by eq. (16).

Fig. 2. *Two soliton collision on a tilted plane:* Solution of eq. (1), for $l_{\text{chain}} = 104$; zero boundary conditions; $V_n = 16n/l_{\text{chain}}$; initial soliton parameters: $\alpha_1 = \pi$, $\alpha_2 = 0.$, $\beta_1 = 0.5$ and $\beta_2 = 0.3$; integration time $T = 90$.

Fig. 3. *Soliton trapped on potential maximum:* Solution of eq. (1), for $l_{\text{chain}} = 104$; periodic boundary conditions; $V_n = 2\cos(2\pi n/l_{\text{chain}})$; initial soliton parameters: $\alpha = -1.571$, $\beta = 0.4$; integration time $T = 90$.

Fig. 4. *Soliton trapped on an attractive impurity:* Solution of eq. (1), for $l_{\text{chain}} = 314$; periodic boundary conditions; $V_n = V\delta_{n,0}$, $V = -0.3$; initial parameters: $\alpha = 0.$, $\beta = 0.4$; integration time $T = 30.$; $|\psi|$-magnification: 2.

Fig. 5. *Soliton trapped on a repulsive impurity:* Solution of eq. (1), for $l_{\text{chain}} = 314$; periodic boundary conditions; $V_n = V\delta_{n,0}$, $V = 0.67$; initial soliton parameters: $\alpha = 0.$, $\beta = 1.0$; integration time $T = 90$.

Fig. 6. *Soliton on a strong, repulsive impurity:* Solution of eq. (1), for $l_{\text{chain}} = 314$; periodic boundary conditions; $V_n = V\delta_{n,0}$, $V = 0.70$; initial soliton parameters: $\alpha = 0.$, $\beta = 1.0$; integration time $T = 90$.

Fig. 7. *Soliton in a periodic potential:* Solution of eq. (1), for $l_{\text{chain}} = 500$; periodic boundary conditions; $V_n = \frac{1}{10}\cos(2\pi n/25)$; initial soliton parameters: $\alpha = 0.5$, $\beta = 0.1$; integration time $T = 180.$; $|\psi|$-magnification: 10.

Fig. 8. *Slow soliton in a random, weak potential:* Solution of eq. (1), for $l_{\text{chain}} = 500$; periodic boundary conditions; $V_{\text{max}} = 0.1$; initial soliton parameters: $\alpha = 0.3$, $\beta = 0.1$; integration time $T = 90.$; $|\psi|$-magnification: 10.

Fig. 9. *Fast soliton in a random, weak potential:* Solution of eq. (1), for $l_{\text{chain}} = 500$; periodic boundary conditions; $V_{\text{max}} = 0.1$; initial soliton parameters: $\alpha = 1.57$, $\beta = 0.1$; integration time $T = 90.$; $|\psi|$-magnification: 10.

Fig. 10. *The "double-sine-map":* phase plane for the map (27) with $K = T = 2$.

Fig. 11. *Soliton moving in a regular region:* $K = -T = -2.$, $q_0 = 2\pi/10$, $p_0 = 0$; 50 iterations forward and backward; length of the bars corresponds to δq_n, the spread of the solution in q-direction at time n.

Fig. 12. *Soliton moving in a chaotic region:* $K = T = 2.$, $q_0 = \pi/100$, $p_0 = 0$; 50 iterations forward and backward.

Fig. 13. *Full dynamics versus collective variable approximation:* $\pi(p_{n+1} - p_n)/K$ versus q_n compared with $\sin q_n$ for the chaotic case shown in Fig. 12.

Fig. 14. *Time-reversal for "regular" soliton:* Spread $\delta q_n/\pi$ versus n; time reversal at $n = 50$; initial condition same as in Fig. 11.

Fig. 15. *Time-reversal for "chaotic" soliton:* Spread $\delta q_n/\pi$ versus n; time reversal at $n = 50$; initial condition same as in Fig. 12.

Fig. 1

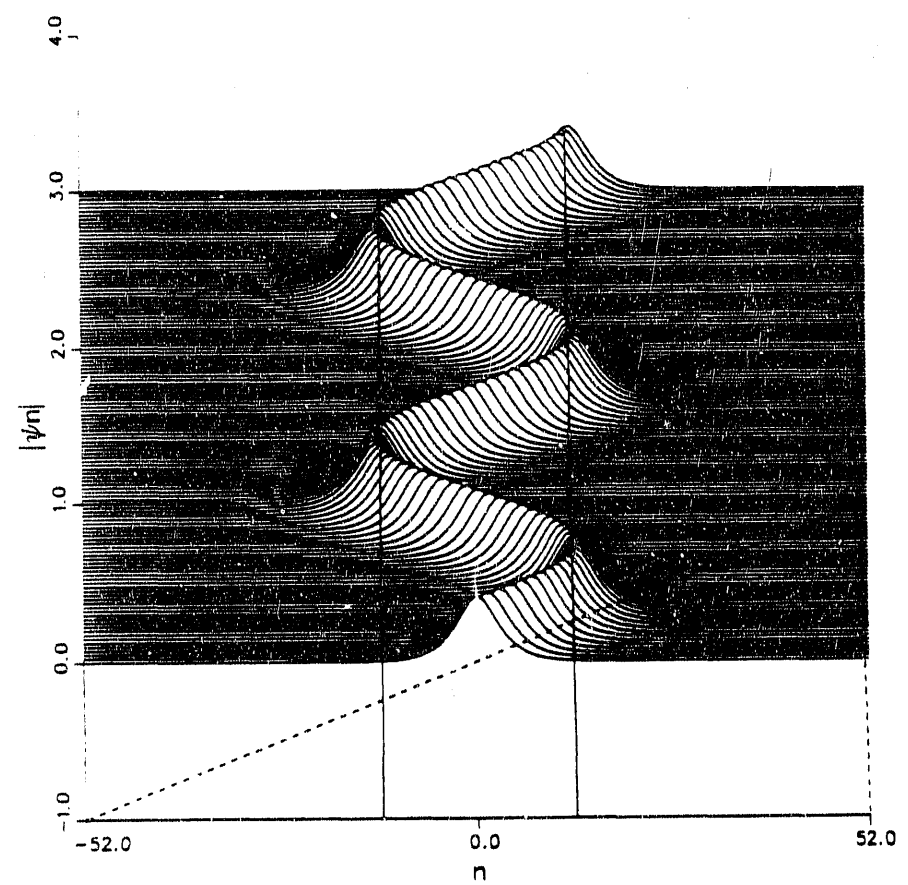

Integrable NLS chain

Zero b. c.

Chain length = 104.

alpha = −1.571

beta = 0.400

Vmax = 8.000

tend = 90.00

tol*e+3 = 0.00100

Fig. 2

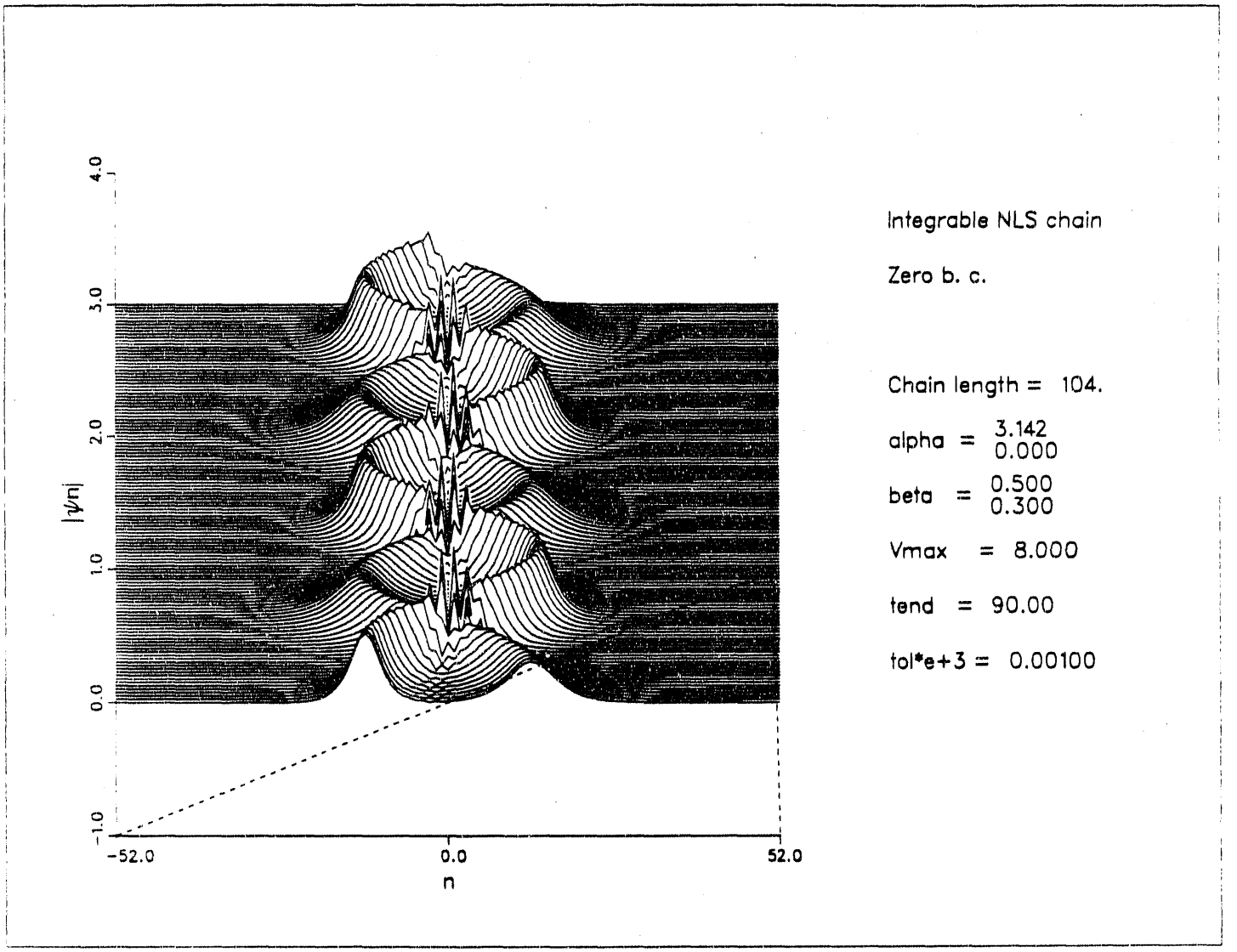
4.0
3.0
2.0
1.0
0.0
-1.0
|ψn|
-52.0
0.0
52.0
n
Integrable NLS chain
Zero b. c.
Chain length = 104.
alpha = 3.142 / 0.000
beta = 0.500 / 0.300
Vmax = 8.000
tend = 90.00
tol*e+3 = 0.00100

Fig. 3

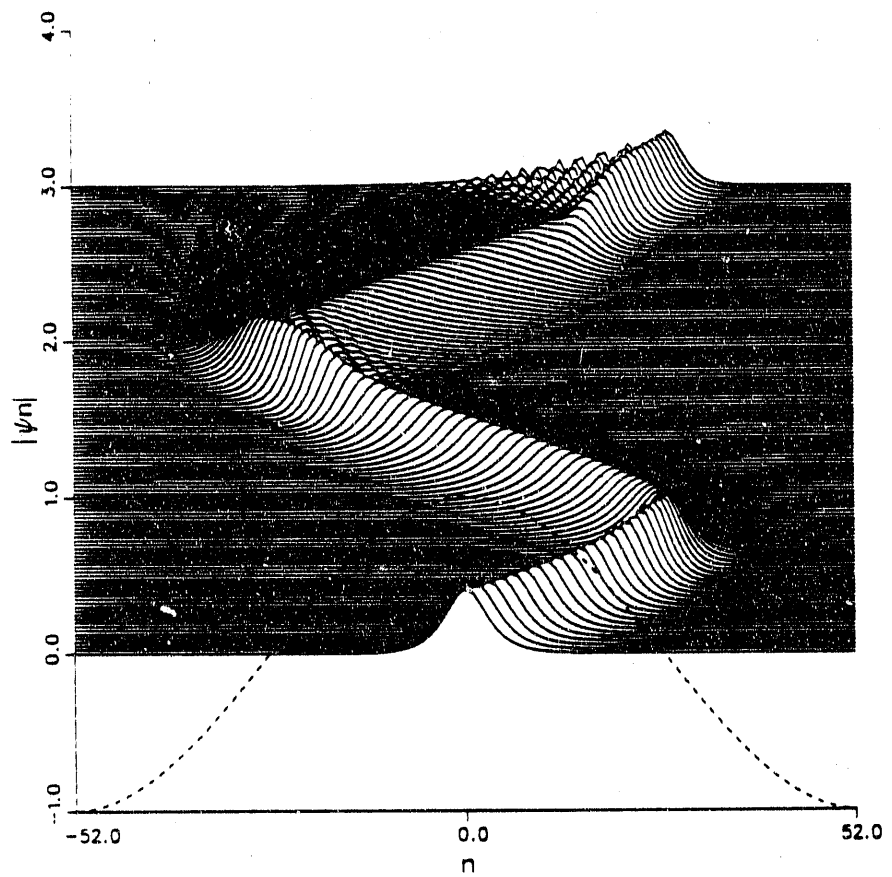

Integrable NLS chain

Periodic b. c.

Chain length = 104.

alpha = −1.571

beta = 0.400

Vmax = 2.000

tend = 90.00

tol*e+3 = 0.00100

Fig. 4

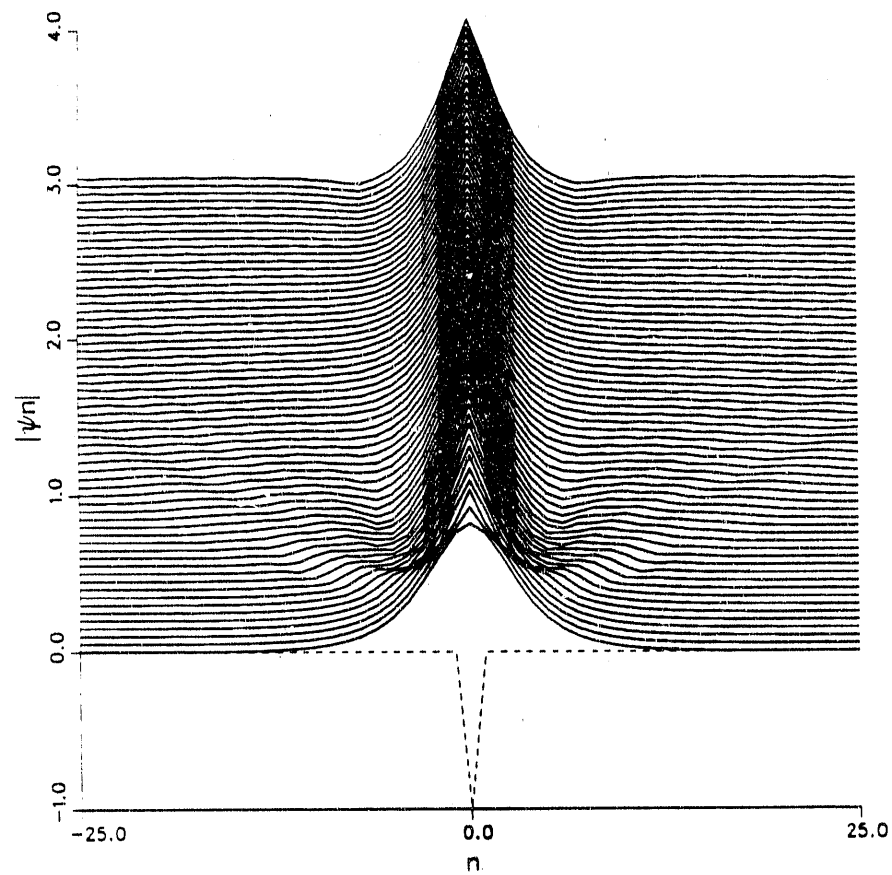

Integrable NLS chain (attrac.)

Periodic b. c.

Chain length = 314

alpha = 0.000

beta = 0.400

Vmax = 0.3000

LV = −1.0000

tend = 30.00

tol = 1.e−6

y−magn. = 2.0

Fig. 5

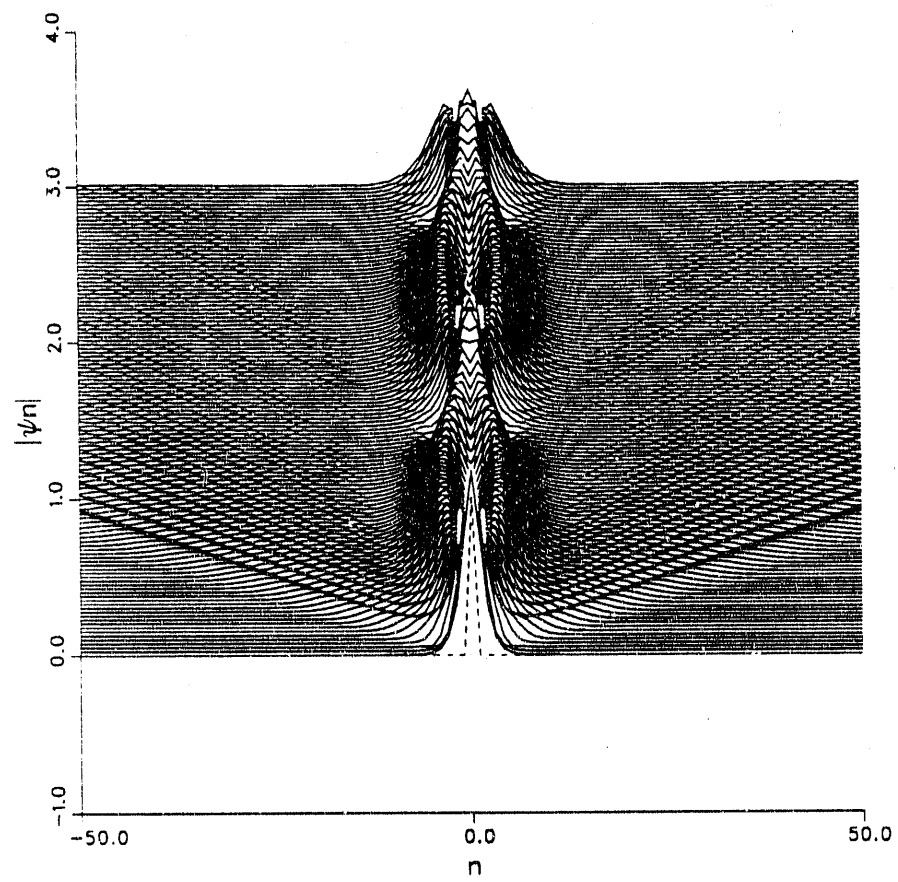

Integrable NLS chain (attrac.)

Periodic b. c.

Chain length = 314

alpha = 0.000

beta = 1.000

Vmax = 0.6700

LV = −1.0000

tend = 90.00

tol = 1.e−6

Fig. 6

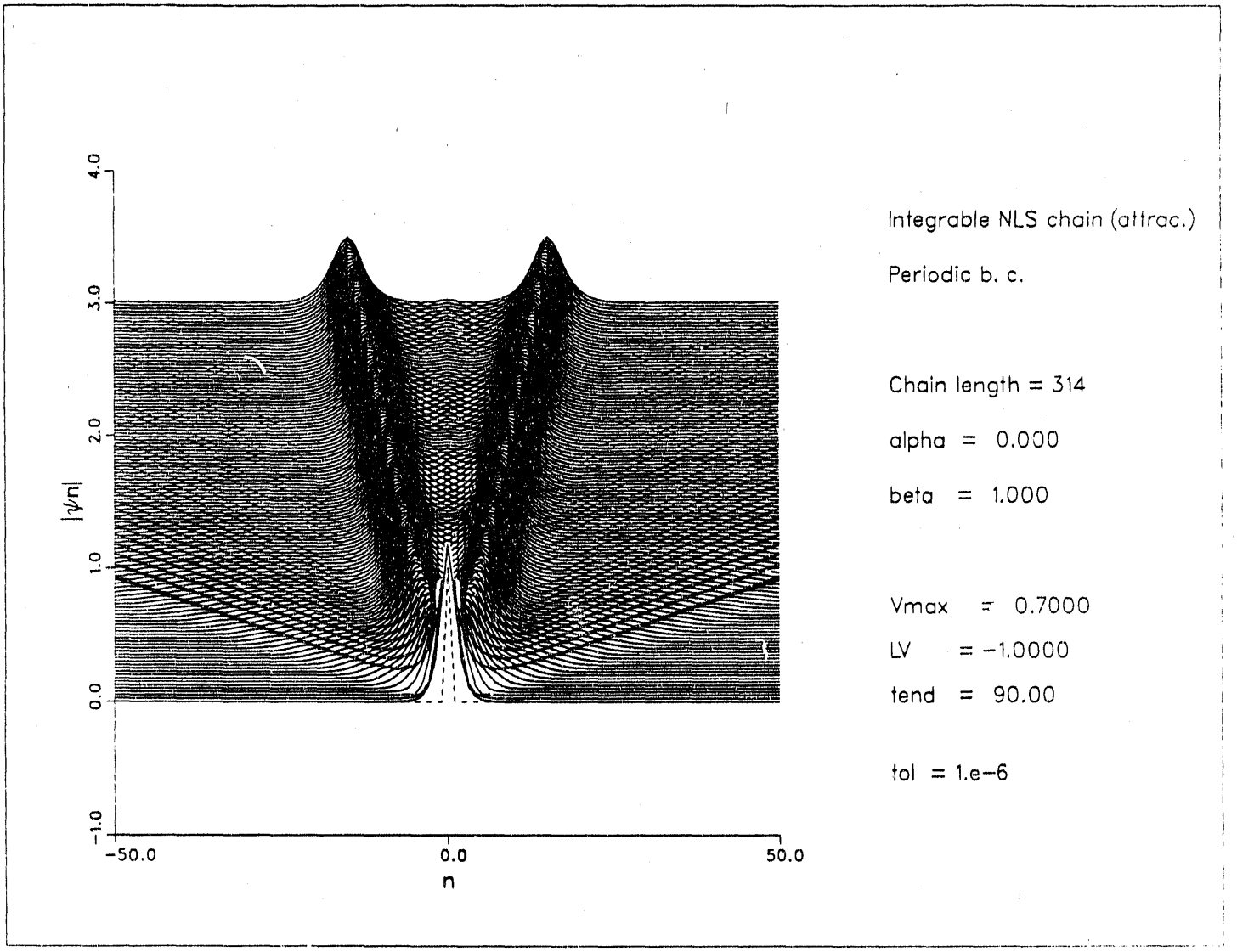
4.0
3.0
2.0
1.0
0.0
-1.0
|ψn|
-50.0
0.0
50.0
n
Integrable NLS chain (attrac.)
Periodic b. c.
Chain length = 314
alpha = 0.000
beta = 1.000
Vmax = 0.7000
LV = −1.0000
tend = 90.00
tol = 1.e−6

Fig. 7

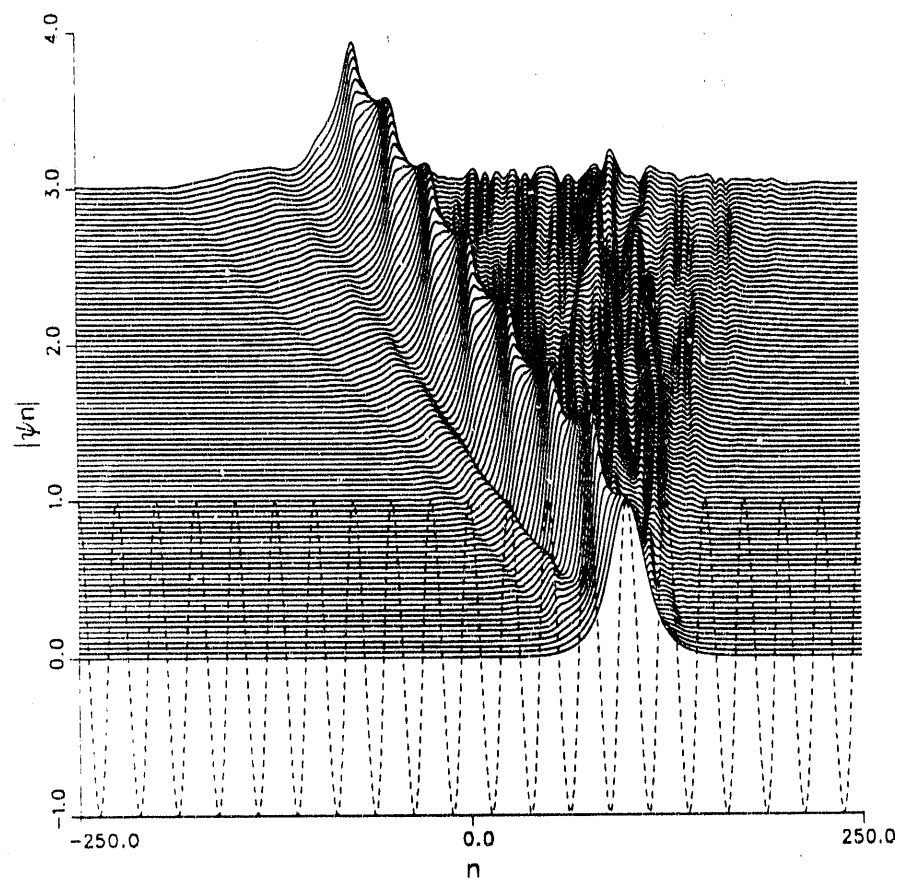

Integrable NLS chain (attrac.)

Periodic b. c.

Chain length = 500

alpha = 0.500

beta = 0.100

Vmax = 0.1000

LV = 25.0000

tend = 180.00

tol = 1.e−6

y−magn. = 10.0

Fig. 8

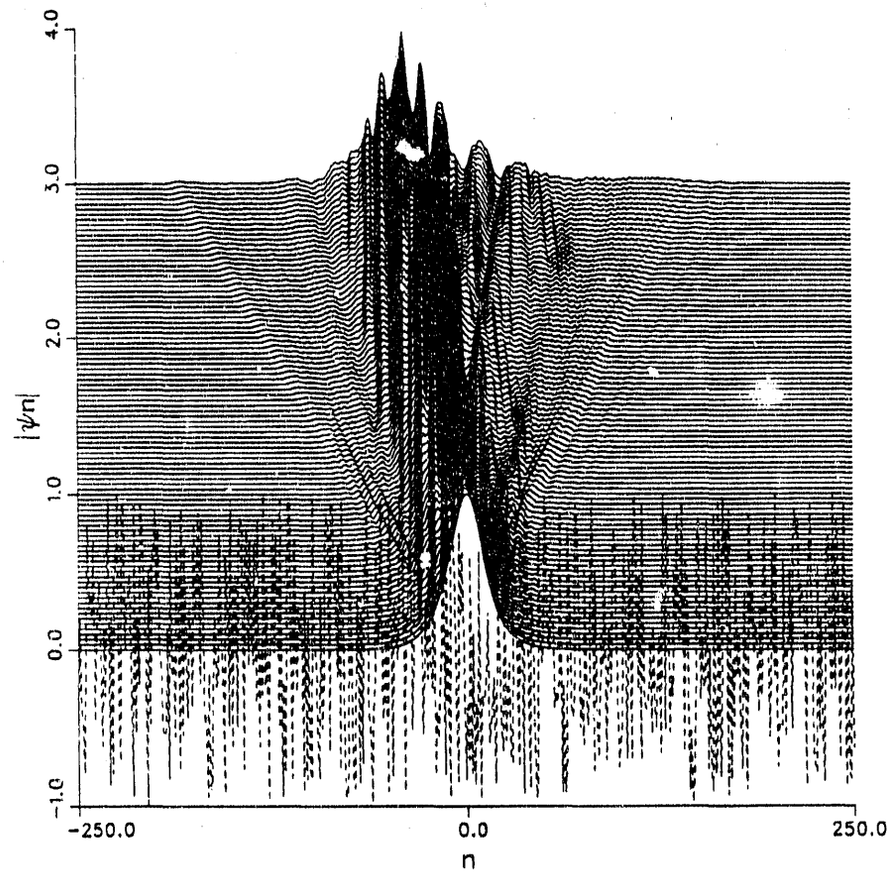

Integrable NLS chain (attrac.)

Periodic b. c.

Chain length = 500

alpha = 0.300

beta = 0.100

Vmax = 0.0999

random pot.

tend = 90.00

tol = 1.e-6

y-magn. = 10.0

Fig. 9

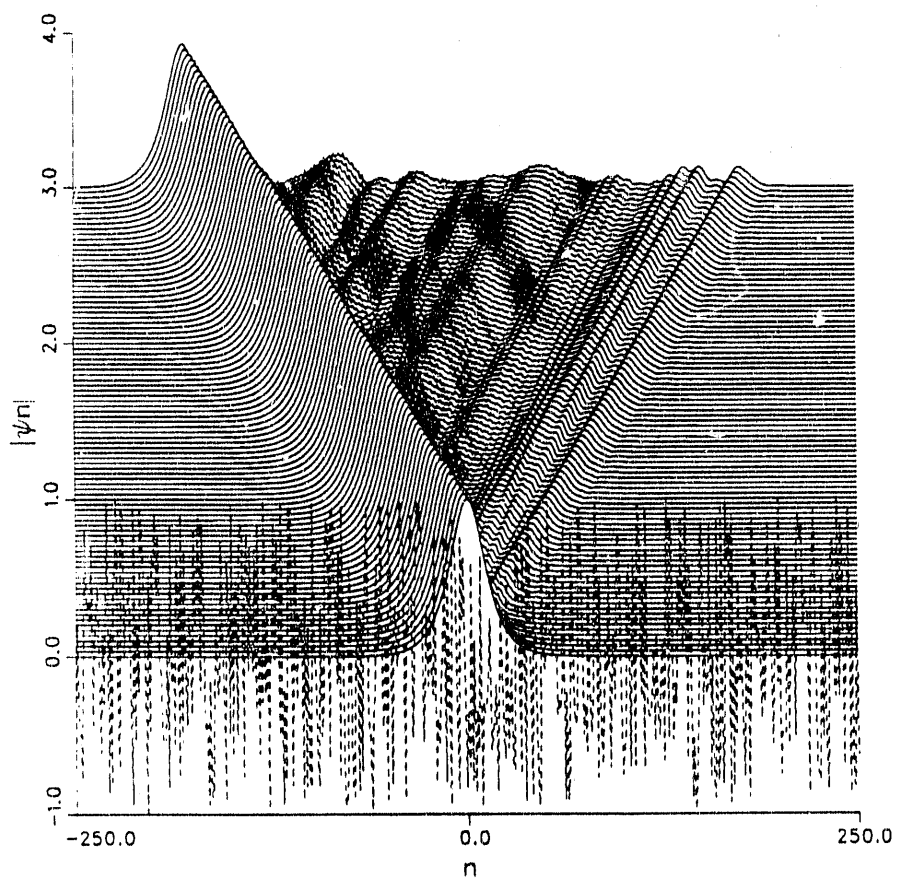

Integrable NLS chain (attrac.)

Periodic b. c.

Chain length = 500

alpha = 1.570

beta = 0.100

Vmax = 0.0999

random pot.

tend = 90.00

tol = 1.e-6

y-magn. = 10.0

Fig. 10

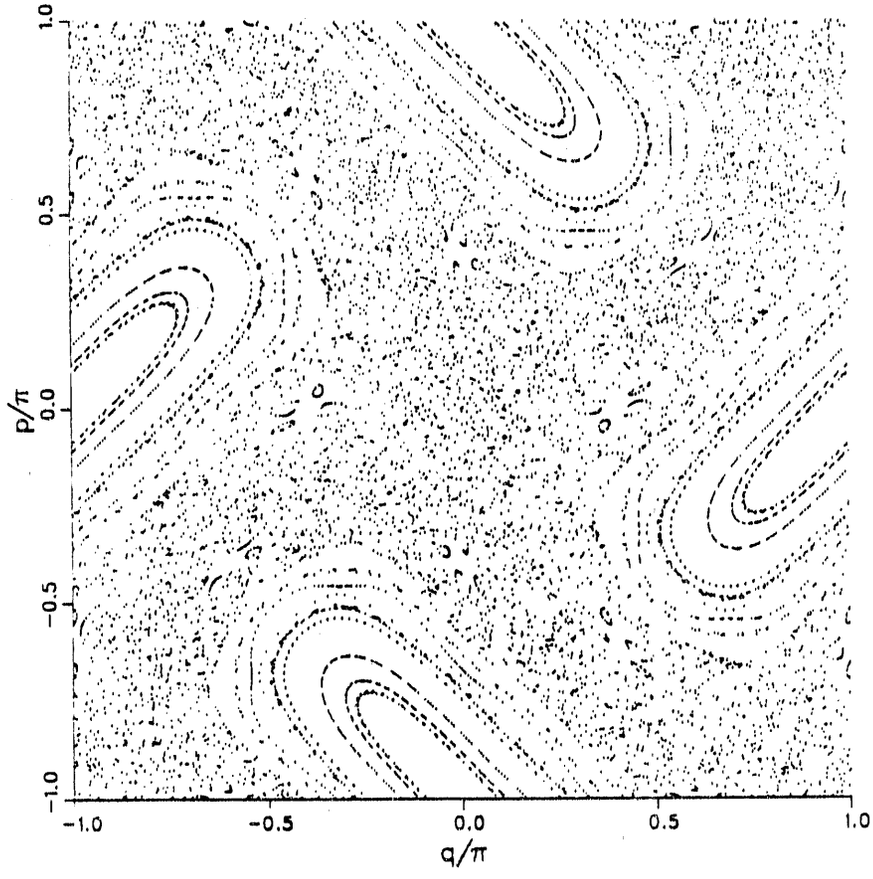

K = 2.000

T = 2.000

Fig. 11

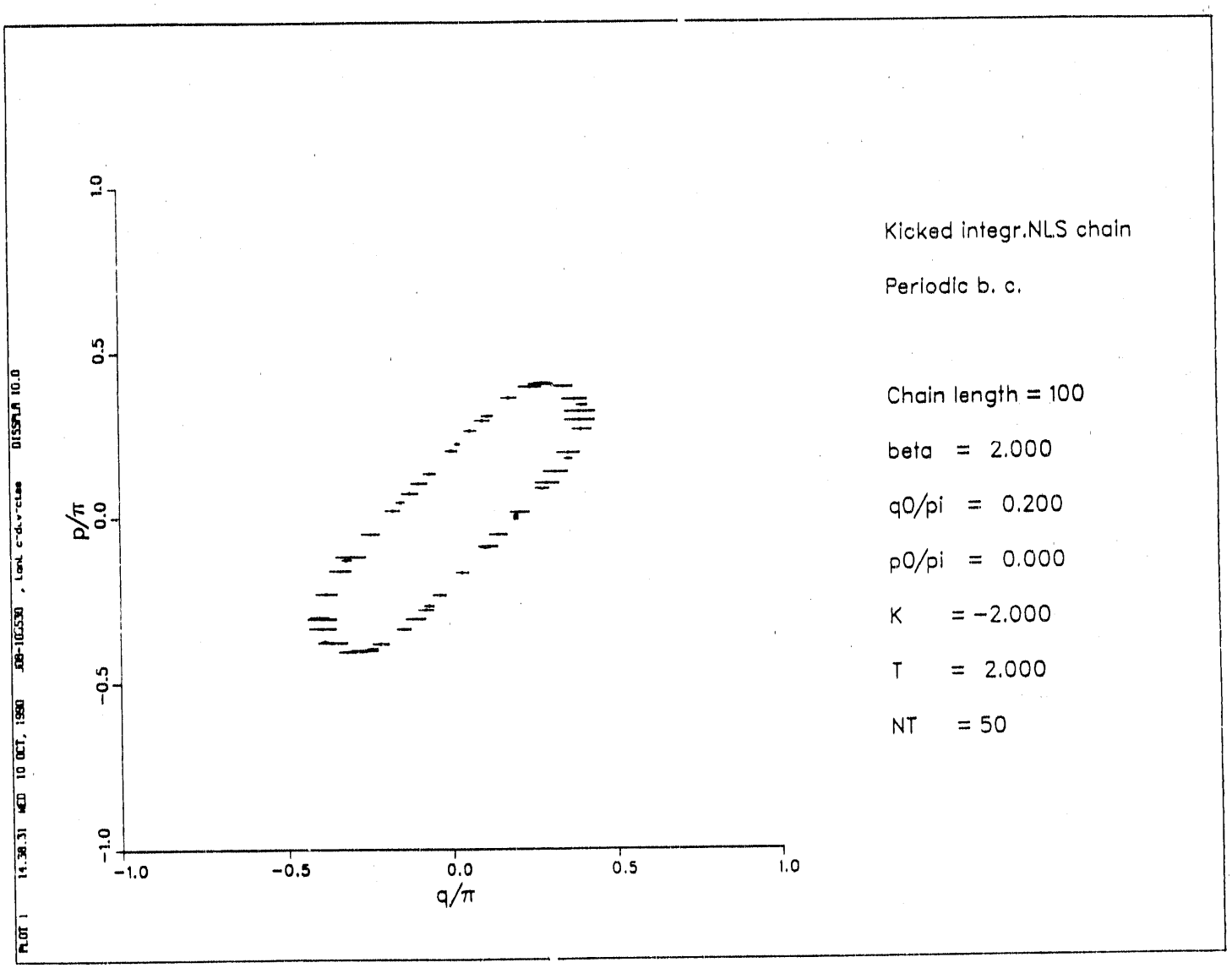
Kicked integr.NLS chain
Periodic b. c.
Chain length = 100
beta = 2.000
q0/pi = 0.200
p0/pi = 0.000
K = −2.000
T = 2.000
NT = 50
p/π
q/π
1.0
0.5
0.0
−0.5
−1.0
−1.0
−0.5
0.0
0.5
1.0

Fig. 12

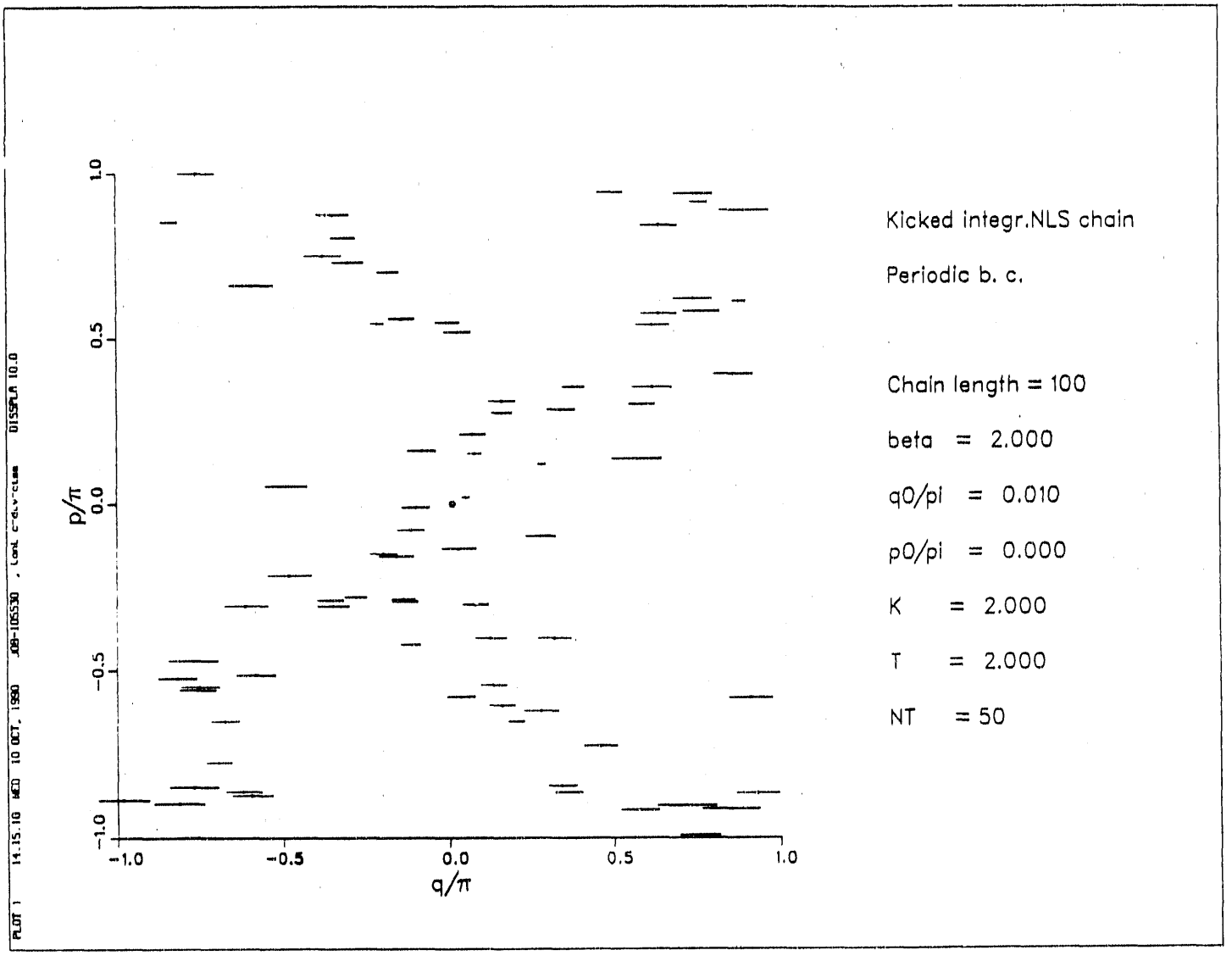
p/π
q/π
1.0
0.5
0.0
-0.5
-1.0
-1.0
-0.5
0.0
0.5
1.0
Kicked integr.NLS chain
Periodic b. c.
Chain length = 100
beta = 2.000
q0/pi = 0.010
p0/pi = 0.000
K = 2.000
T = 2.000
NT = 50

Fig. 13

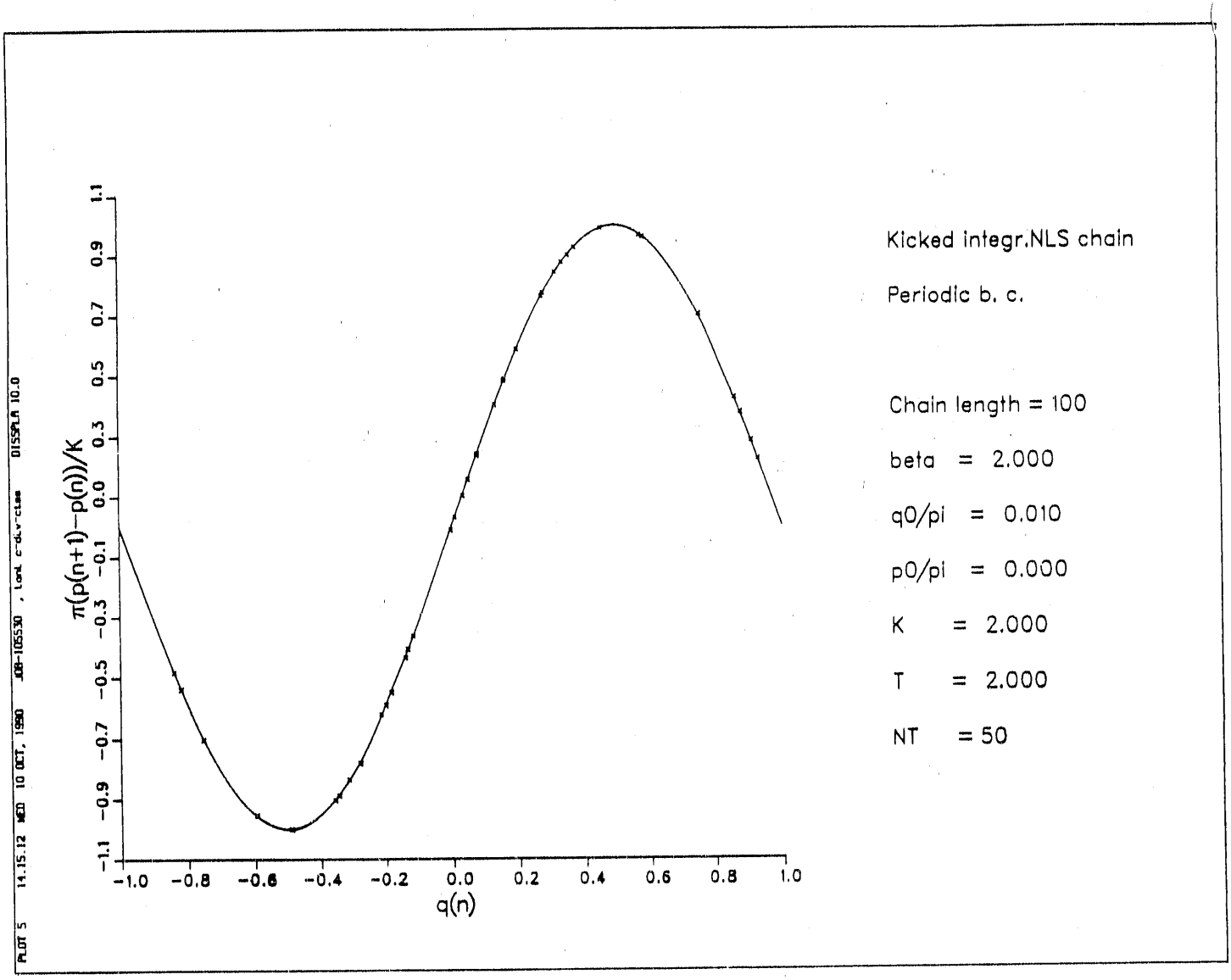
π(p(n+1)−p(n))/K
q(n)
−1.1 −0.9 −0.7 −0.5 −0.3 −0.1 0.0 0.3 0.5 0.7 0.9 1.1
−1.0 −0.8 −0.6 −0.4 −0.2 0.0 0.2 0.4 0.6 0.8 1.0
Kicked integr.NLS chain
Periodic b. c.
Chain length = 100
beta = 2.000
q0/pi = 0.010
p0/pi = 0.000
K = 2.000
T = 2.000
NT = 50

Fig. 14

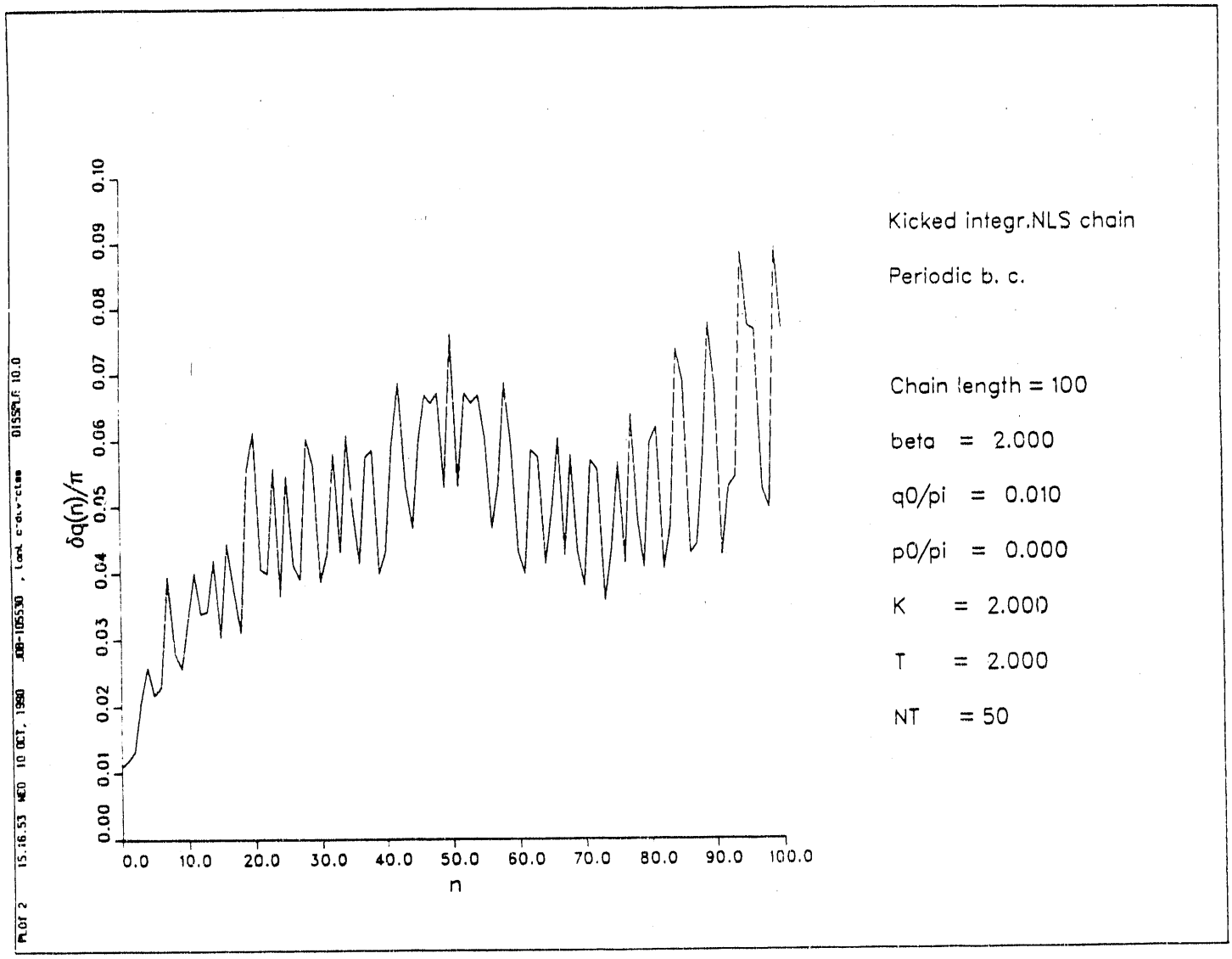
δq(n)/π
0.00
0.01
0.02
0.03
0.04
0.05
0.06
0.07
0.08
0.09
0.10
0.0
10.0
20.0
30.0
40.0
50.0
60.0
70.0
80.0
90.0
100.0
n
Kicked integr.NLS chain
Periodic b. c.
Chain length = 100
beta = 2.000
q0/pi = 0.010
p0/pi = 0.000
K = 2.000
T = 2.000
NT = 50

Fig. 15

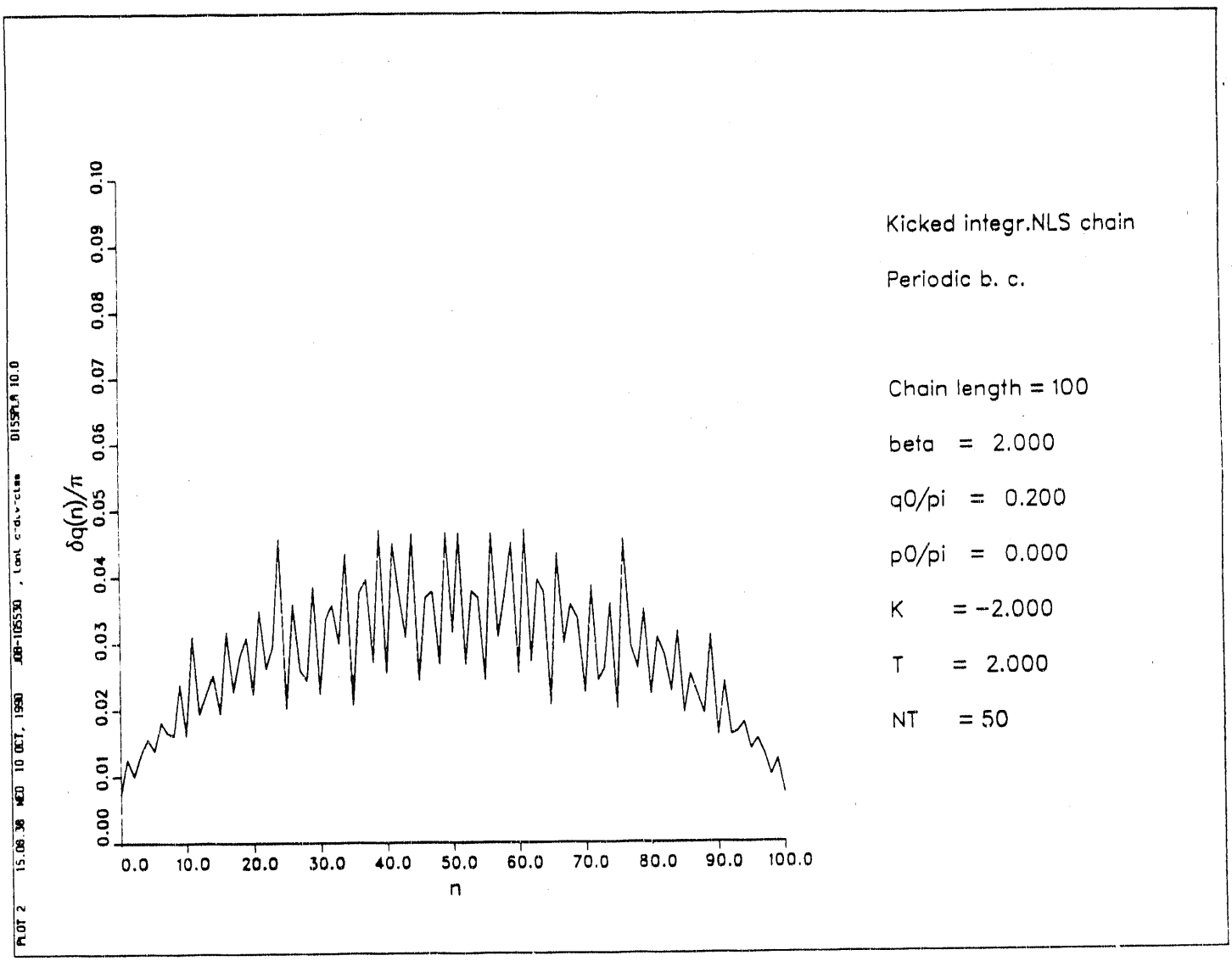
PLOT 2 15.08.38 WED 10 OCT, 1980 JOB-105530 , tant c-d-v-clas DISSPLA 10.0
δq(n)/π
0.00 0.01 0.02 0.03 0.04 0.05 0.06 0.07 0.08 0.09 0.10
0.0 10.0 20.0 30.0 40.0 50.0 60.0 70.0 80.0 90.0 100.0
n
Kicked integr.NLS chain
Periodic b. c.
Chain length = 100
beta = 2.000
q0/pi = 0.200
p0/pi = 0.000
K = -2.000
T = 2.000
NT = 50

END

DATE FILMED

01 / 31 / 91